Stability and elastic properties of hydrogen-loaded $Ti_{1-x}Al_x$ alloys: An *ab initio* study

P. Jund, W. Zhong, and D. Tománek
Department of Physics and Astronomy and Center for Fundamental Materials Research, Michigan State University, East Lansing, Michigan 48824-1116
(Received 1 August 1994)

In order to improve our understanding of hydrogen embrittlement occurring in $Ti_{1-x}Al_x$ alloys, we calculated the equilibrium structure and the elastic constants of bulk Ti, Al, the ordered alloy Ti_3Al, as well as their hydrides, using the *ab initio* density functional formalism. Complementary results of calculations for ordered systems, substitutional impurities, and small clusters reproducing defect geometries show that hydrogen loading leads to a reduction of the *shear* modulus of $Ti_{1-x}Al_x$ alloys. We found that on the electronic level, the softened shear response is reflected in a valence charge depletion in the (0001) planes of the Ti-based lattice, which occurs only when both Al and H are present. These results shed light on the problem of why fracture is facilitated upon hydrogen loading of metallic Ti containing Al impurities.

I. INTRODUCTION

Titanium is a very important metal in industry due to the diversity of its usage in marine, aerospace, and medical implant technology. The wide range of its applicability arises chiefly from the very large strength-to-weight ratio of Ti. It is also well known that the strength and other mechanical properties of this system improve significantly upon alloying titanium with aluminum, in a fashion comparable to the improved elastic behavior of steel caused by the presence of carbon in the iron matrix. Unfortunately, the ductility of the titanium aluminides Ti_3Al and TiAl is very low below 600 °C. Moreover, the mechanical stability of $Ti_{1-x}Al_x$ alloys is significantly reduced in the presence of hydrogen.[1]

Many experimental and theoretical studies have been performed during the last 20 years (for a review, see Ref. 2) with the objective to reduce the brittle behavior of these systems at room temperature, without deteriorating their advantageous elastic behavior at elevated temperatures. These studies have established that the origin of the low ductility at room temperature lies in the hindrance of motion of specific dislocations due to their pinning,[3] and that this effect is related to the flow stress anomaly found in TiAl single crystals.[4]

Two theoretical calculations have addressed the pinning of dislocations in the stoichiometric TiAl alloys, both of which relate this effect to the covalent bonding in these systems. Greenberg and co-workers have shown that the anisotropy of the charge density near the Ti atoms in TiAl causes a many-valleyed Peierls relief which could affect the mobility of dislocations.[5] More recently, Morinaga and co-workers found a strong Ti $3d$–Al $3p$ bonding between the (001) planes of the TiAl alloy,[6] which may lie at the origin of the large value of the shear modulus C_{44}, determined by Fu and Yoo.[7] Further alloying with $3d$ transition metals might reduce this strong Ti $3d$–Al $3p$ bonding, thereby enhancing the mobility of dislocations and hence the ductility of TiAl.

The objective of our study is to understand the mechanical properties of the more dilute $Ti_{1-x}Al_x$ systems and the corresponding alloys containing hydrogen.[8] Even at low Al concentrations, the hydrogen-free $Ti_{1-x}Al_x$ alloys show an increased strength as compared to pure Ti. Unfortunately, this increased strength is accompanied by an enhanced propensity towards stress-corrosion cracking (SCC) in aqueous solutions[1,9] as well as organic liquids.[10]

Our discussion will focus on the transgranular (rather than the intergranular) cracking mechanism which dominates especially at larger Al concentrations used in high-strength alloys. Even though the onset of transgranular fracture can be influenced by many factors, the reduced stress resistance has been traced back in many cases to hydrogen uptake by the metal. Presence of hydrogen has been found to cause significant strength reductions in Ti alloys containing as little as 5% (weight) of Al.[9] It is interesting to note that the pure Ti metal, which forms a stable hydride, is not susceptible to hydrogen-induced transgranular stress-corrosion cracking, and neither are Ti-Al alloys containing less than 2% (weight) Al. It has also been observed that with increasing Al concentration in Ti, the nature of dislocation motion changes from tangled or cellular to a coplanar slip at essentially the same composition which marks the onset of the susceptibility towards transgranular stress-corrosion cracking.[11]

These observations raise a number of issues which have to be addressed. The first basic question is whether the adverse effect of hydrogen on the mechanical stability of $Ti_{1-x}Al_x$ alloys with $x > 2\%$ has a predominantly electronic origin, reflected in the change of local bonding [in a way similar to the effect of H on the stability of Pd (Ref. 12)], or rather a structural origin, related to a propensity towards structural transitions.

An indication in favor of the electronic origin are the significantly different electronic configurations and electronegativities of Al and Ti, implying a large charge transfer between these species in the alloy. The interrelationship between the charges carried by the atoms and

mechanical failure has been demonstrated by a successful application of cathodic potentials to inhibit transgranular cracking.[13]

On the other hand, $Ti_{1-x}Al_x$ is not a random alloy even at the low Al concentrations associated with the onset of hydrogen embrittlement; at higher Al concentrations and temperatures the propensity towards the formation of the intermetallic compound Ti_3Al has been observed. This, together with the fact that the crystalline structures of the pure components are different, would rather speak in favor of a structural origin of stress-corrosion cracking. Hence one of the first questions to be asked is whether it is predominantly electronic or structural effects which lie at the root of hydrogen-induced stress-corrosion cracking in these systems.

To our knowledge, no theoretical information is available on the electronic and structural properties of $Ti_{1-x}Al_xH_y$ alloys, whereas several studies have been performed on Ti hydrides.[14] We have made use of three different yet complementary *ab initio* techniques in order to elucidate different aspects of hydrogen embrittlement in $Ti_{1-x}Al_x$ alloys at various compositions. The objective of our studies is not to compare the range of applicability of these techniques, but rather to obtain a detailed and reliable description of the bonding changes in the $Ti_{1-x}Al_x$ matrix in the vicinity of hydrogen.

A summary of the theoretical methods, which have been described in more detail elsewhere, will be presented in the following Sec. II. Results regarding the pure metals Al and Ti will be given in Sec. III. In Sec. IV, we present results for the hydrogen-free $Ti_{1-x}Al_x$ alloys, and in Sec. V for these alloys with dissolved hydrogen. We discuss our results in Sec. VI and present our conclusions in Sec. VII.

II. THEORY

We determine the equilibrium geometry, the total energy, and the electronic structure of hydrogen-free and hydrogen-loaded $Ti_{1-x}Al_x$ alloys using different implementations of the density-functional formalism within the local-density-approximation (LDA).[15] In the electronic ground state, the total energy functional is minimized by solving self-consistently the set of Kohn-Sham equations[15]

$$\left[-\frac{\hbar^2}{2\,m}\nabla^2 + V_{\rm ion} + V_H + V_{\rm xc}\right]\psi_{n\vec{k}} = \epsilon_{n\vec{k}}\psi_{n\vec{k}} \qquad (1)$$

and

$$\rho(\vec{r}) = \sum_{n\vec{k}}^{\rm occ} |\psi_{n\vec{k}}(\vec{r})|^2 \,. \qquad (2)$$

Here, $V_{\rm ion}$ is the potential due to the ion cores, for which we use either the all-electron potential or an *ab initio* pseudopotential. V_H is the Hartree potential and $V_{\rm xc}$ is the exchange-correlation potential associated with the electron density $\rho(\vec{r})$, which we use in the form parametrized by Hedin and Lundqvist.[16] $\psi_{n\vec{k}}$ and $\epsilon_{n\vec{k}}$ are the Kohn-Sham wave functions and energies, respectively. The crystal momentum $\vec{k}$ is used only in the case of ordered alloys. The wave functions are expanded in a local basis, containing atom-centered and floating orbitals, and the angular momentum is limited to $l_{\rm max} = 2$ in all our calculations. The total energy of the system in the electronic ground state is calculated using

$$E_{\rm tot} = \sum_{n\vec{k}}^{\rm occ} \epsilon_{n\vec{k}} - \frac{1}{2}\int d\vec{r}\; V_H(\rho(\vec{r}))\rho(\vec{r}) - \int d\vec{r}\; V_{\rm xc}(\rho(\vec{r}))\rho(\vec{r})d\vec{r} + \int d\vec{r}\; \epsilon_{\rm xc}[\rho(\vec{r})]\rho(\vec{r}) + E_{\rm ion-ion}\,, \qquad (3)$$

where $\epsilon_{\rm xc}[\rho(\vec{r})]\rho(\vec{r})$ is the exchange-correlation energy density and $E_{\rm ion-ion}$ describes the interaction between ion cores.

In order to obtain reliable values for the equilibrium lattice parameters and the elastic constants of the different compounds, we fitted the total energy to a Morse potential. To insure an accurate fit, we performed six to eight total energy calculations per compound, using lattice constants within a 10% range around the equilibrium value.

A. Calculations for ordered bulk alloys

To calculate the electronic properties of ordered bulk alloys, we use the pseudopotential local-orbital method which has been discussed in detail previously and which has been applied successfully to transition metals and their hydrides.[12,17] The interaction of valence electrons with the ion cores is described by first-principles pseudopotentials $V_{\rm ion}$ of the Hamann-Schlüter-Chiang type.[18] The Gaussian local-orbital basis functions

$$f_{\alpha lm}(\vec{r}) = A_{\alpha lm}e^{-\alpha r^2}K_{lm}(\theta,\phi) \qquad (4)$$

are centered on atomic sites, and are also used as floating orbitals at interstitial sites. The Kubic harmonics K_{lm} represent the angular part of the basis functions, and $A_{\alpha lm}$ are normalization constants. The Brillouin zone, which is defined in ordered crystalline solids, is sampled by a homogeneous mesh of special $\vec{k}$ points.[19]

B. Calculations for ordered solids with impurities

To obtain the charge distribution around an impurity dissolved in an otherwise unperturbed medium we use the linear muffin tin orbitals (LMTO)-Green function method within the atomic sphere approximation (ASA). This is an all-electron technique which is used within the frozen-core approximation. In the multiple scattering theory, the local density of states at each location $\vec{r}$ in the alloy is given by the imaginary part of the Green function $G(\vec{r},\vec{r},E)$. It has been well established how,

within the LMTO scheme, this function can be obtained from the structural Green function $\Gamma(E)$,[20] which is related to the Green function of the pure host $\bar{\Gamma}(E)$ by the Dyson equation

$$\Gamma_{LL'}^{nn'}(E) = \bar{\Gamma}_{LL'}^{nn'}(E) - \sum_{n'',L''} \bar{\Gamma}_{LL''}^{nn''}(E) \triangle P_{l''}^{n''}(E) \Gamma_{L''L'}^{n''n'}(E) . \quad (5)$$

Here, n labels the site, $L = (l, m)$ the orbital symmetry, and $\triangle P_{l''}^{n''}(E)$ describes the local perturbation at the site n'' due to the presence of the defect. Sites at which $\triangle P_{l''}^{n''}(E)$ is nonzero define the perturbed cluster. Due to the good screening in metals, the perturbation is essentially confined within the nearest neighbor shell of the impurity site, which justifies the selection of these sites as the perturbed cluster in our calculations. We perform the calculations using the simple diagonal cluster (SDC) model in which the intersite Green function matrix elements of the pure host $\bar{\Gamma}_{LL''}^{nn''}(E)$ $(n \neq n'')$ are neglected in Eq. (5). The SDC approximation, while reducing the computing time by one order of magnitude, has been shown to yield results which are very close to those obtained by an exact solution of Eq. (5).[20]

In our calculations, we assume that all atoms have a spherical muffin-tin potential within their Wigner-Seitz sphere, and that the radius of these overlapping spheres is the same at all the sites in the alloy. Since the screening, which occurs outside the perturbed cluster in response to the impurity, does not change significantly the charge distributions in the perturbed cluster, we ignored this screening effect in our calculation.

C. Cluster calculations

In order to closely investigate the local impact of hydrogen on the metallic bonding in Ti-Al systems with no symmetry restrictions, we used a cluster implementation of the density functional formalism in the DMOL code.[21] The molecular orbitals are represented by linear combinations of numerically generated basis functions. In the double-numerical basis set,[21] the occupied valence orbitals are represented by two wave functions each. The basis is expanded at each site using polarization functions with angular momentum quantum number which is higher by 1 than the highest angular momentum in the free atom. We use the frozen core approximation to treat the inner core electrons and the von Barth and Hedin potential to describe the exchange-correlation energy.[22]

III. PURE CONSTITUENTS

A. Aluminum

Even though the electronic structure of Al has been studied previously,[23] we include our corresponding results for the sake of completeness and comparison with Al-based alloys.

The energy of the Al pseudoatom amounts to $E_{\rm tot}^{\rm atom}({\rm Al}) = -65.562$ eV, which includes the calculated spin-polarization energy of -0.178 eV. The $3s$ and $3p$ valence orbitals are represented by three radial Gaussian functions each, with the optimized decays (in a.u.) $\alpha = 0.10, 0.28, 0.80$, yielding 12 independent basis functions at each site. In our bulk calculation, the Fourier expansion of the charge density is truncated at an energy of 49 Ry, and the irreducible part of the Brillouin zone is sampled by 60 $\vec{k}$ points.

The calculated properties of bulk Al in the face-centered-cubic (fcc) phase, which are summarized in Table I, are in excellent agreement with experimental data.[24] We find bulk aluminum to be slightly overbound,[25] due to the well known underbinding of atoms in the LDA. The total density of states[26] (TDOS) of Al, shown in Fig. 1(a), exhibits the nearly parabolic behaviour near the lower valence band edge, as expected for a near-free-electron metal. We found these results to lie very close to our parallel calculations using a plane-wave basis and the all-electron LMTO method, indicating the convergence and interchangeability of these techniques.

B. Titanium

The analogous calculations for Ti yield the value $E_{\rm tot}^{\rm atom}(Ti) = -89.963$ eV for the total energy of the iso-

TABLE I. Calculated and observed ground-state properties of bulk Al, Ti, Ti_3Al, and their hydrides: lattice constant a, cohesive energy (with respect to isolated atoms) $E_{\rm coh}$, bulk modulus B, and shear modulus C_{44}.

		Al	Ti(fcc)	Ti(hcp)	Ti_3Al	AlH	TiH	TiH_2	Ti_3AlH_4
a (a.u.)	LDA[a]	7.80	7.73	5.55	7.76	8.25	8.19	8.63	8.14
	Expt.	7.66	7.73	5.58	7.68			8.41	8.22
$E_{\rm coh}$ (eV)	LDA[a]	−3.51	−3.70	−3.70	−15.15	−4.99	−6.15	−8.81	−24.19
	Expt.	−3.39	−4.70	−4.70					
B (GPa)	LDA[a]	71	94	100	280	70	72	74	290
	Expt.	73	106	106					
C_{44} (GPa)	LDA[a,b]	37		43	101	15	52		67
	Expt.	32		46					

[a]Given are results obtained using the *ab initio* pseudopotential local orbital method. Results obtained using the LMTO-ASA method are discussed in Ref. 24.

[b]Calculations are for shear within the (0001) plane, along the [1000] direction [see Fig. 9(c)].

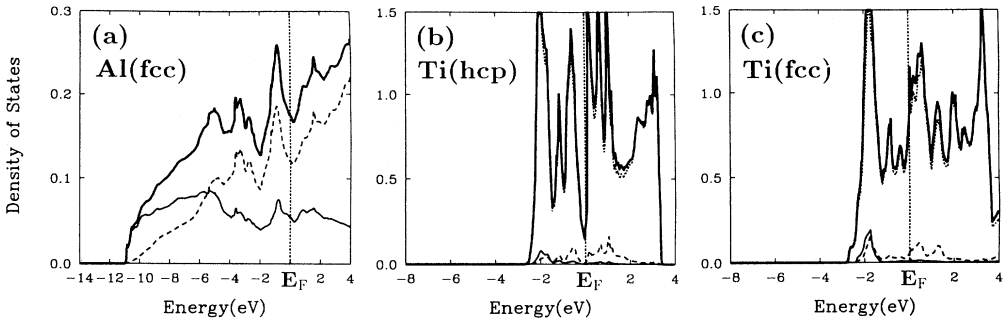

FIG. 1. Electronic density of states of bulk (a) Al(fcc), (b) Ti(hcp), and (c) Ti(fcc), calculated using *ab initio* pseudopotentials and a local-orbital basis. The bold solid line gives the total density of states, the solid line the partial density of states (PDOS) of s electrons, the dashed line the PDOS of p electrons, and the dotted line the PDOS of d electrons. Note the different vertical scales used in (a), (b), and (c).

lated pseudoatom. The Ti atom contains both localized $3d$ and delocalized $4s$ electrons, which can only be described by relatively deep pseudopotentials. In our calculation, the $3d$, $4s$, and $4p$ valence orbitals are represented by four radial functions each, with the optimized Gaussian decays (in a.u.) $\alpha = 0.18$, 0.56, 1.79, and 5.70. Hence our basis contains 40 independent functions at each Ti site.

The equilibrium structure of Ti at low temperatures is hexagonal close packed (hcp), which differs from the fcc structure only in the stacking sequence of the close-packed layers ($ABAB$ in hcp vs $ABCABC$ in fcc). Since all coordination numbers and hence the packing fractions in the two structures are the same, we expect the total energy and the electronic structure of Ti in these two structures to be very similar. This is indeed confirmed by the results of our calculations, given in Table I and Figs. 1(b) and 1(c). The gain of symmetry (and consequently reduction of the computing requirements) in the cubic structure more than compensates for the small error introduced when considering the fcc in lieu of the hcp phase.

These bulk results are based on a cutoff of the Fourier expansion of the charge density and potential at an energy of 49 Ry, and a sampling of the irreducible part of the Brillouin zone by 27 $\vec{k}$ points in the hcp phase and 60 $\vec{k}$ points in the fcc phase. Our results for the electronic structure of Ti in the hcp structure lie close to the LMTO results, obtained using 196 $\vec{k}$ points in the irreducible wedge of the Brillouin zone, in particular reproducing the pronounced depression in the density of states near E_F discussed below.

A close inspection of the structural data, presented in Table I, confirms the high precision with which the LDA predicts the equilibrium geometry of bulk Ti. As suggested above, the binding energies of Ti in the hcp and the fcc phases are nearly the same,[25] and found to be indistinguishable in our LDA calculations. Our total energies, on the other hand, underestimate the cohesion of Ti in comparison with the experimental data. In view of the computational difficulties traditionally associated with the nonlocal $3d$ pseudopotentials, we checked the convergency of these results by augmenting the basis set by interstitial floating orbitals, and by extending the Fourier cutoff energy from 49 Ry to 100 Ry, but found the total energy to be affected by less than 0.1 eV. More important to us is the elastic response of Ti where, in the case of the bulk modulus, the LDA results are in close agreement with the experimental data.

The small difference between Ti in the hcp and the fcc structures is reflected in the electronic densities of states, which are presented in Figs. 1(b) and 1(c), respectively.

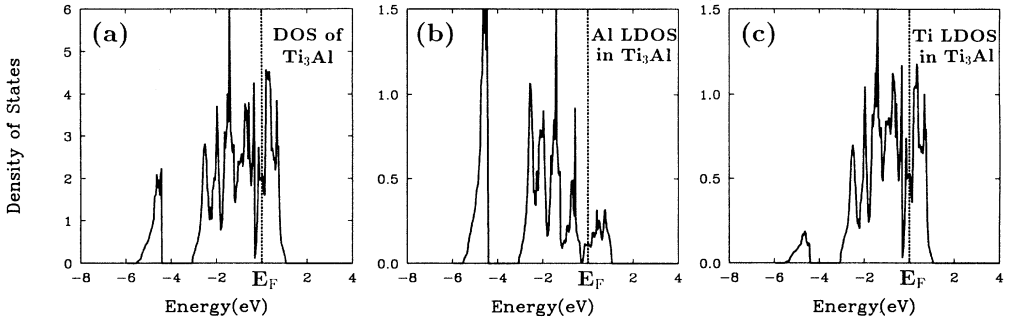

FIG. 2. Electronic density of states of the ordered bulk alloy Ti_3Al in the cubic phase, calculated using *ab initio* pseudopotentials and a local-orbital basis. (a) Total density of states per Ti_3Al formula unit, (b) the local density of states (LDOS) at the Al site, and (c) the LDOS at the Ti site. Note the different vertical scales used in (a), (b), and (c).

The width of the occupied band $W_{occ} \approx 3$ eV, the total $3d$-band width $W_{tot} \approx 6$ eV, and the three-peak structure of the $3d$ band below the Fermi level are common to both hcp and fcc titanium. The slight stabilization of the hcp with respect to the fcc phase of Ti is reflected in a state depletion in the hcp structure near the Fermi level, which is accompanied by a lowering of the band structure energy.

IV. HYDROGEN-FREE $Ti_{1-x}AL_x$ ALLOYS

Before discussing the adverse effect played by hydrogen on the elastic behavior of high-strength $Ti_{1-x}Al_x$ alloys, we discuss in detail the electronic structure of the hydrogen-free ordered alloy Ti_3Al, and compare the results to those for a substitutional Al impurity in Ti(hcp).

A. Ordered alloy Ti_3Al

We discuss the ordered compound Ti_3Al, since the presence of this phase in high-strength titanium alloys has been linked to their increased susceptibility towards transgranular cracking.[27] The close-packed structure of Ti_3Al which we consider has an underlying simple cubic (sc) Bravais lattice, and can be obtained from the metastable fcc phase of Ti by replacing the corner sites in the conventional unit cell by Al atoms. This structure, which is very closely related to that of the experimentally observed hcp stacked system,[28] has significantly higher symmetry and hence can be computationally treated with a higher precision. Our basis contains Ti- and Al-centered orbitals, as discussed in the preceding section. We found our results to be well converged when sampling the irreducible part of the Brillouin zone by 20 $\vec{k}$ points, and when using an energy cutoff of 49 Ry in the Fourier expansion of the charge density.

The negative value of the formation energy of Ti_3Al,[29] reported in Table II, indicates stability with respect to decomposition into pure Ti and Al metals. The calculated and observed equilibrium structural properties, as well as the bulk modulus, of Ti_3Al are summarized in Table I.[25] The experimental value given for the lattice constant a of Ti_3Al in the metastable cubic phase has been obtained by extrapolating the experimental data for the hexagonal phase,[30] assuming that the unit cell volume is the same in the cubic and the hexagonal structures. This value is in good agreement with our calculated equilibrium lattice constant.

The electronic density of states of the ordered Ti_3Al alloy,[26] calculated using *ab initio* pseudopotentials and a local-orbital basis, is presented in Fig. 2(a). The site-projected local electronic densities of states (LDOS's) on the Al and Ti sites are given in Figs. 2(b) and 2(c), respectively. When comparing this density of states to that of the pure bulk constituents Al and Ti in Fig. 1, we notice the formation of a new hybrid band located ≈ 5 eV below the Fermi level, with a bandwidth of about 1 eV. The angular momentum decomposition shows that this band has predominantly an Al $3s$–Ti $3d$ character; a comparison between the local densities of states in Figs. 2(b) and 2(c) indicates a predominant localization of these states on the Al sites. The presence of new occupied Al-derived states is consistent with the Mulliken population analysis, reported in Table III, which indicates a net transfer of as much as 0.9 electrons from Ti to the Al sites.

TABLE II. Formation energies E_{form} (eV) (Refs. 29, 31) of $Ti_{1-x}Al_xH_y$ systems.

Ti_3Al	AlH	TiH	TiH_2	Ti_3AlH_4
−0.54	0.87	−0.10	−0.40	0.45

TABLE III. Mulliken excess charges (e^-) on individual sites in $Ti_{1-x}Al_xH_y$ systems.

	AlH	TiH	TiH_2	Ti_3Al	Ti_3AlH_4
Ti	0.28	0.08	0.30	0.65	
Al	0.70			−0.89	0.43
H	−0.70	−0.28	−0.04		−0.59

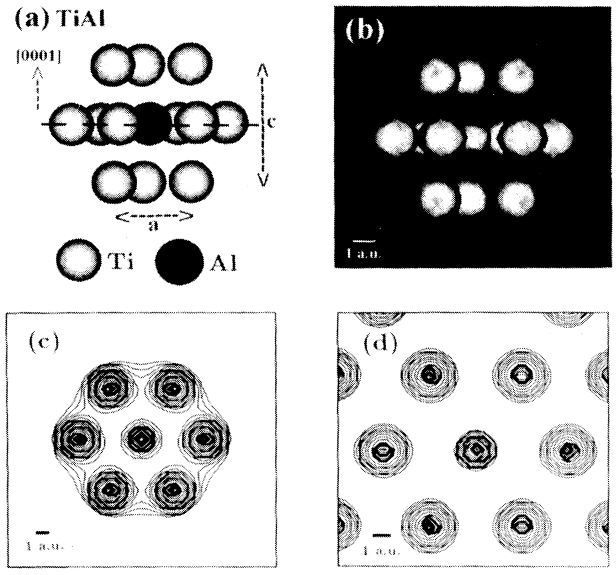

FIG. 3. Geometry and charge distribution in a very dilute TiAl alloy, represented by Ti(hcp) with a substitutional Al impurity. (a) Geometry of the $Ti_{12}Al$ core cluster. (b) Three-dimensional (3D) representation of the total charge density surface in the $Ti_{12}Al$ cluster, corresponding to $\rho = 0.1\ e^-/\text{a.u.}^3$, calculated using the DMOL all-electron cluster method. (c) Results of the same calculation, presented as a 2D contour plot in the (0001) plane, which is shown by the dashed line in (a) and contains the Al impurity. (d) Total charge density in the dilute TiAl alloy, calculated using the LMTO–ASA–Green-function method, and represented in the same manner and geometry as in (c). The ratio of two consecutive contours in (c) and (d) is $\rho(n+1)/\rho(n) = 1.5$.

B. Al impurities in Ti

In order to understand the effect of aluminum on the electronic structure of $Ti_{1-x}Al_x$ alloys even at very low Al concentrations, we performed calculations for a substitutional Al impurity in a pure Ti(hcp) matrix. We placed all the atoms on a perfect Ti(hcp) lattice, given by the experimentally observed lattice parameters ($a = 5.577$ a.u. and $c/a = 1.588$). In the LMTO-ASA calculation, we assumed the same mean radius for all the overlapping atomic Wigner-Seitz spheres, and considered the perturbed cluster, consisting of the Al impurity and its 12 nearest neighbors [see Fig. 3(a)], to be embedded in an otherwise perfect crystal. These results were compared to those obtained applying the DMOL approach to the isolated $Ti_{12}Al$ core cluster, frozen in the bulk geometry.

A three-dimensional representation of the total charge density within the isolated $Ti_{12}Al$ core cluster is shown in Fig. 3(b). A two-dimensional contour plot of the charge density in the (0001) plane containing the Al impurity, indicated by a dashed line in Fig. 3(a), is presented in Fig. 3(c) for the isolated cluster and in Fig. 3(d) for the Ti matrix with a single Al impurity. A comparison of the results in Figs. 3(c) and 3(d) indicates that the isolated cluster gives a good idea of the electronic structure near a substitutional Al impurity in bulk Ti.

The local densities of states on the Al impurity and on its nearest Ti neighbors, obtained using the LMTO-ASA approach, are shown in Figs. 4(a) and 4(b), respectively. Our analysis of the net charges on the Al impurity and its Ti neighbors, presented in Table III, yields a consistent picture with results obtained in the ordered Ti_3Al alloy. As seen in Fig. 4(a), the substitutional Al impurity induces a sharp resonant state near the bottom of the valence band, about 7 eV below the Fermi level. This state is mainly localized on the Al site and nearly invisible at the neighboring Ti sites and, in the ordered Ti_3Al alloy, spreads out to the (Al $3s$–Ti $3d$)-derived band discussed above. As in the ordered alloy, the Al site is negatively charged. The LMTO-ASA calculation yields for the total charge on the Al site the value of 0.18 electrons, which compares well with the Mulliken charge of 0.22 electrons on the Al site in the isolated $Ti_{12}Al$ cluster, yet is significantly smaller than the value in the ordered Ti_3Al alloy.

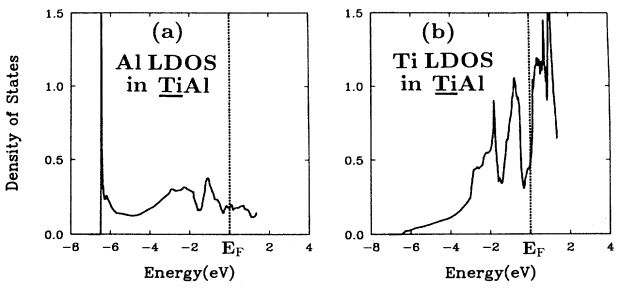

FIG. 4. Electronic structure of a very dilute TiAl alloy, represented by Ti(hcp) with a substitutional Al impurity, calculated using the LMTO–ASA–Green function method. The local density of states at (a) the Al site and (b) the neighboring Ti site is given by the solid line.

V. HYDROGEN-LOADED $Ti_{1-x}Al_x$ ALLOYS

In an attempt to enhance our understanding of the microscopic origin of hydrogen embrittlement in $Ti_{1-x}Al_x$ alloys, we calculated the structural and electronic properties of bulk Al, Ti, and Ti_3Al at different hydrogen concentrations, with the hydrogen atoms located in the interstitial sites of the lattice.

The basis functions on the metal atom sites have been described above. Hydrogen atoms in a crystalline environment are represented by 16 independent basis functions. The radial dependence of the basis functions with s and p symmetry is given by four Gaussians each, with the decay constants (in a.u.) $\alpha = 0.20, 0.42, 0.68$, and 1.36.[12] We use the same $\vec{k}$ point sampling of the irreducible Brillouin zone and the same energy cutoff of the Fourier expansion of the charge density in hydrogen-loaded as in hydrogen-free systems.

A. AlH

It is well known experimentally that hydrogen is not readily absorbed in metallic aluminum.[8] For the sake of completeness of our study, nevertheless, and in order to demonstrate the adequacy of our computational scheme, we present in the following results for a hypothetical compound AlH, where the H atoms occupy the octahedral interstitial sites in the fcc lattice of aluminum.

The positive calculated value for the formation energy of AlH,[31] given in Table II, agrees indeed with the experimental finding that AlH should be unstable. Our predictions for the other structural properties of AlH are reported in Table I. These results suggest that the bulk modulus of AlH should be nearly the same as that of pure Al, whereas the shear modulus C_{44} of Al would be expected to decrease by more than 50% in the hydride. As shown in Table III, this change of the elastic response is accompanied by a large transfer of 0.7 electrons from the Al to the H sites.

B. TiH_x

In contrast to aluminum, bulk titanium does form stable hydrides.[8] As mentioned above, we constrain our structural optimization of TiH_x to the fcc phase, and compare our results to those for Ti(fcc). Guided by available information,[8] we place the hydrogen atoms at the octahedral and tetrahedral interstitial sites of the fcc lattice.

We first consider the ordered compound TiH, where hydrogen atoms occupy all the available octahedral sites, as shown in Fig. 5(a). The observed readiness of Ti to absorb hydrogen is reflected in a negative value of the formation energy of TiH,[31] given in Table II. The structural properties of TiH are summarized in Table I. Our results indicate an expansion of 6% of the lattice constant of Ti upon hydrogen uptake, in general agreement with lattice dilatations observed in compact metallic structures.[8] Results of our Mulliken population analysis, reported

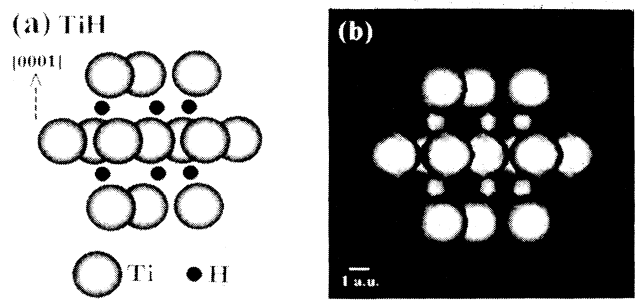

FIG. 5. Geometry and charge distribution in TiH, with hydrogen atoms occupying the octahedral interstitial sites of the hcp lattice. (a) Geometry of a $Ti_{13}H_6$ core cluster. (b) 3D representation of the total charge density surface in the $Ti_{13}H_6$ cluster, corresponding to $\rho = 0.1\ e^-/\text{a.u.}^3$, calculated using the DMOL all-electron cluster method.

in Table III, suggest a small positive charge on the Ti atoms. The total charge density, calculated for the isolated $Ti_{13}H_6$ core cluster [see Fig. 5(a)] using the DMOL formalism, is presented in Fig. 5(b).

Next we consider the compound TiH_2, where all the hydrogen atoms occupy the tetrahedral interstitial sites of the fcc lattice, yielding a fluorite structure of the system. As shown in Table II, the calculated formation energy[31] of TiH_2 is negative and lower than that of TiH. This is in agreement with experimental results which suggest that transition metal elements of the groups 3B, 4B, and partly those of group 5B tend to form dihydrides.[32] The structural properties of TiH_2, summarized in Table I, suggest a further expansion of the lattice with respect to TiH, yet essentially the same compressibility as the monohydride.

We find that our calculated total density of states $N(E)$ of TiH_2, shown in Fig. 6(b), lies very close to augmented plane wave (APW) results for the same system.[33] In particular, our value of the density of states at the Fermi level[26] $N(E_F) = 1.76$ states/eV compares very well with the APW value $N(E_F) = 1.73$ states/eV.[33] A comparison between the local density of states on the Ti sites in TiH_2, shown in Fig. 6(c), with the density of states of pure Ti, reproduced in Fig. 6(a), suggests that the Ti-H interaction strongly modifies the Ti $3d$ band and induces a new (Ti $3d$–H $1s$)-derived band about 5 eV below E_F. This new H-induced band is split into two subbands due to the close proximity of the two hydrogen atoms in the unit cell. The overscreening of the proton charge on the H sites, reported in Table III, is much smaller than in TiH, and agrees well with previous results.[34]

C. $Ti_{1-x}Al_xH_y$

In order to better understand the adverse effect of hydrogen on the binding in $Ti_{1-x}Al_x$ alloys, we performed density functional calculations for the ordered compound Ti_3AlH_4 in the simple cubic structure. We compared these results to those for the hydride of a very dilute TiAl alloy, represented by an isolated $Ti_{12}AlH_6$ core cluster shown in Fig. 7(a). Even though the simple cubic structure of the ordered alloy may not correspond to the equilibrium phase of this system, we selected it for its high symmetry and for the sake of simple comparison with our results for the hydrogen-free Ti_3Al compound. As in TiH and AlH, we assumed that the hydrogen atoms occupy all the octahedral interstices in this structure, four in number in the conventional unit cell of the fcc lattice which coincides with the unit cell of Ti_3AlH_4. We expect our results for this system to elucidate the conjugate roles played by both H *and* Al in the embrittlement of Ti-based systems.

The calculated positive value of the formation energy of Ti_3AlH_4, given in Table II, indicates a potential instability of this system towards decomposition into its components in their standard state. This may be the reason why no structure has been observed or reported for this system.[35] The calculated structural properties, summarized in Table I, show among others that the LDA slightly underestimates the experimental equilibrium lattice constant of related systems.[35] The compactness of this structure is reflected in the large value of the bulk modulus. We also note the substantial decrease of the

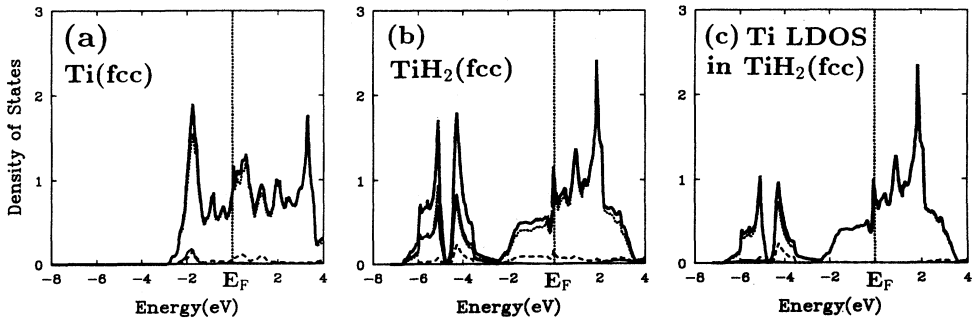

FIG. 6. Comparison of electronic densities of states in bulk Ti and TiH_2. (a) Density of states of Ti(fcc), (b) density of states of TiH_2(fcc), and (c) local density of states on the Ti site in TiH_2(fcc), calculated using *ab initio* pseudopotentials and a local-orbital basis. The bold solid line gives the total density of states, the solid line the partial density of states (PDOS) of s electrons, the dashed line the PDOS of p electrons, and the dotted line the PDOS of d electrons.

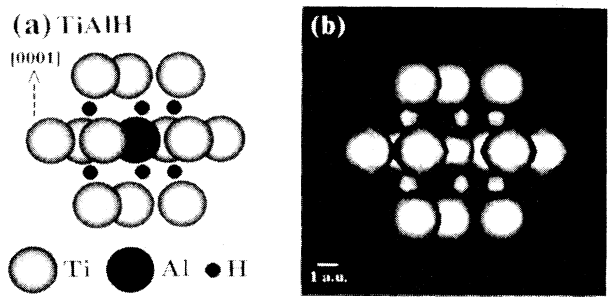

FIG. 7. Geometry and charge distribution in the hydride of a very dilute TiAl alloy, represented by a Ti(hcp) matrix with a substitutional Al impurity and hydrogen atoms occupying the octahedral interstitial sites of the hcp lattice. (a) Geometry of a $Ti_{12}AlH_6$ core cluster. (b) 3D representation of the total charge density surface in the $Ti_{12}AlH_6$ cluster, corresponding to $\rho = 0.1\ e^-/\text{a.u.}^3$, calculated using the DMOL all-electron cluster method.

shear modulus C_{44} of this system with respect to the hydrogen-free structure.

The calculated total density of states[26] of bulk Ti_3AlH_4 is compared to that of the hydrogen-free Ti_3Al system in Fig. 8. The corresponding results of the Mulliken population analysis for these bulk compounds are reported in Table III. The most prominent difference in Ti_3AlH_4 with respect to the hydrogen-free compound is a significant charge reversal on the Al site. We find the Al atoms to carry a net positive charge in the presence of hydrogen, whereas they carry a net negative charge in the hydrogen-free Ti_3Al alloy. On the other hand, independent of hydrogen concentration, the net charge on the Ti atom is always positive, whereas that on the H site is always negative.

The calculated total charge density of the hexagonal $Ti_{12}AlH_6$ cluster [see Fig. 7(a)] is presented in Fig. 7(b). These calculations confirm the inversion of the net charge on the Al site, depending on the presence or absence of hydrogen in the cluster. The total energy difference

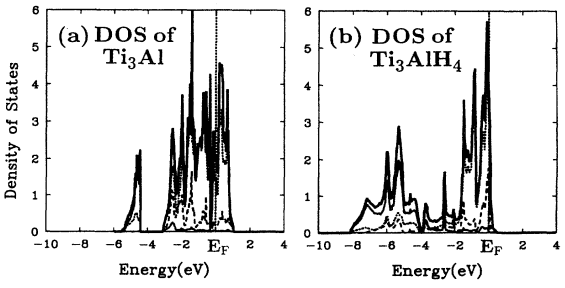

FIG. 8. Comparison of the total electronic densities of states in bulk (a) Ti_3Al(fcc) and (b) Ti_3AlH_4, calculated using *ab initio* pseudopotentials and a local-orbital basis. The bold solid line gives the total density of states, the solid line the partial density of states (PDOS) of s electrons, the dashed line the PDOS of p electrons, and the dotted line the PDOS of d electrons.

between the hydrogen-loaded and hydrogen-free $Ti_{12}Al$ clusters indicates that hydrogen is likely to be absorbed even in finite $Ti_{1-x}Al_x$ systems, in agreement with experimental observations.[8]

The above results suggest that the hydrogen-induced decrease of the shear modulus in $Ti_{1-x}Al_x$ systems may be correlated with the net charge near the Al site. To further elaborate on this point, we compared in Figs. 9(a) and 9(b) the charge distributions in the highest occupied molecular orbitals (HOMO's, corresponding to the top of the valence band) of $Ti_{13}H_6$ and $Ti_{12}AlH_6$ clusters, respectively. The geometry and the relevant shear directions as well as the gliding planes in these systems are given schematically in Fig. 9(c). The calculated HOMO charge distributions suggest the presence of charge lobes perpendicular to the shear direction in $Ti_{13}H_6$ clusters, but absence of such bonding charge lobes in the $Ti_{12}AlH_6$ clusters. The absence of bonding charge regions between the gliding planes may lie at the origin of the reduced shear modulus in $Ti_{1-x}Al_xH_y$ systems.

VI. DISCUSSION

As already mentioned in the Introduction, hydrogen-induced embrittlement occurring in $Ti_{1-x}Al_x$ alloys is a very complex problem. The basic questions to be answered are (i) what atomic-scale processes are to be associated with embrittlement, (ii) which changes in the electronic structure are most likely to trigger these processes, and (iii) how this information could be used to reduce or inhibit embrittlement in these systems. When addressing these problems, we have to bear in mind that the response of the system to applied stress depends crucially on both the static structure and bonding strength in the system, as well as on the deformation dynamics leading to mechanical failure.

The first basic problem to be addressed is the equilibrium structure of the system on the atomic scale. Of interest is not only the equilibrium geometry of an ordered monocrystalline alloy of a given composition, but also the possibility of phase transitions induced by internal and external stress, phase separation in the bulk, and segregation at grain boundaries if the system is polycrystalline. Due to the importance of defects on the overall stability of the system, adequate attention must be paid to the structure of dislocations (including partial and superdislocations), faulted dipoles, antiphase boundaries, and twin boundaries, and the effect of other defects such as vacancies and substitutional and interstitial impurities on the equilibrium structure.

Even more important than the structure itself is the nature, strength, and anisotropy of interatomic bonding. Of primary interest in the $Ti_{1-x}Al_xH_y$ systems are changes in the electronic structure and the changing interplay between covalency and ionicity of interatomic bonding as a function of composition, in particular near defect sites. Local changes of the electronic structure will affect not only the local radial compressibility and overall strength of interatomic bonds, which is reflected in the bulk modulus, but also other deformation modes of the

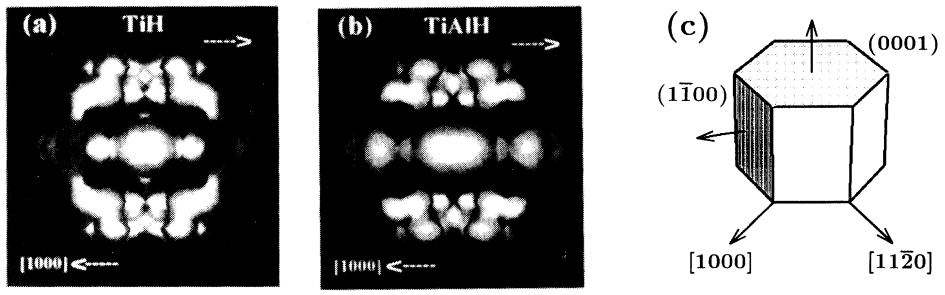

FIG. 9. Charge distribution in the highest occupied molecular orbitals (HOMO's) of (a) $Ti_{13}H_6$ and (b) $Ti_{12}AlH_6$ clusters, both based on the bulk Ti(hcp) structure, calculated using the DMOL all-electron cluster method. A 3D representation of the total charge density surface in (a) and (b) is shown at the value $\rho = 0.001\ e^-/\text{a.u.}^3$. The geometry has been given in Figs. 5(a) and 7(a), respectively. The arrows indicate possible applied shear stress. (c) Schematic drawing of the shear directions and gliding planes in $Ti_{1-x}Al_x$ systems.

system, such as those reflected in the shear modulus. Of particular importance for the overall mechanical stability of the system are such changes near defects and other weak links.

Mechanical deformations under applied stress, which lead to failure, proceed via intergranular and transgranular fracture.[36] The dynamics of the transgranular fracture, which is of main interest in this work, is primarily determined by the ease of Peierls relief and large-scale dislocation motion, both crucially dependent on the potential-energy surfaces and the temperature-dependent mobility of defects (such as interstitial hydrogen) for the structures discussed above. Uncertainty about the atomic-scale processes linked with embrittlement results from the fact that, whereas brittle fracture is typically linked to the inhibition of dislocation motion, processes such as the hydrogen-enhanced local plasticity of a stable system can effectively masquerade as embrittlement on the macroscopic scale.[37–40] This latter process will be discussed in more detail below.

In this study, we attempted to answer some of the above questions by calculating from first principles the equilibrium geometry and stability, the electronic structure, and the elastic response of $Ti_{1-x}Al_xH_y$ systems. We used three different implementations of the *ab initio* density-functional formalism, with no adjustable parameters, in order to compare the electronic structure and bonding strength near defects to those of similar ordered alloys for a wide range of compositions. The computational difficulties for these systems derived from the simultaneous presence of Ti atoms with strongly localized $3d$ electrons, Al atoms with much more delocalized $3s$ and $3p$ electrons, and H atoms with a tendency towards covalent bonding, as well as the large charge transfers between these atoms. We found all our results to be in good agreement with experimental data where available.

Our calculations as well as an inspection of the phase diagram of $Ti_{1-x}Al_x$ alloys indicate that the stability deterioration introduced by aluminum and hydrogen atoms is not caused by local structural rearrangements (phase transitions), but must originate in local changes of interatomic bonding. In the following, we will discuss which changes in the interatomic bonding and the underlying electronic structure were found to correlate with the stability reduction occurring in $Ti_{1-x}Al_x$ alloys upon hydrogen loading. Even though such static considerations have been proven inadequate to describe quantitatively the stability limits of perfect crystals at finite strain,[41] we use them as a first step towards the understanding of the alleged hydrogen embrittlement in these systems.

The first question to be answered is whether the stability of metallic Ti is significantly reduced by the simultaneous presence of Al and H atoms. Our results for the cohesive energies E_{coh} (with respect to isolated atoms), presented in Table I, indicate that presence of hydrogen stabilizes all the metallic systems. This is true when comparing $E_{\text{coh}}(\text{TiH})$ and $E_{\text{coh}}(\text{TiH}_2)$ to $E_{\text{coh}}(\text{Ti})$, $E_{\text{coh}}(\text{AlH})$ to $E_{\text{coh}}(\text{Al})$, and $E_{\text{coh}}(\text{Ti}_3\text{AlH}_4)$ to $E_{\text{coh}}(\text{Ti}_3\text{Al})$. Among these systems, we found the allegedly brittle Ti_3AlH_4 compound to be most stable, and hence brittle behavior to anticorrelate with increasing stability. Our results for the formation energies E_{form} (with respect to the elements in the standard state), presented in Table II, indicate that also the presence of Al in Ti leads to a stable $Ti_{1-x}Al_x$ alloy, even though hydrogen would prefer to be close to the Ti sites in systems with low hydrogen concentrations. The Mulliken population analysis in Table III indicates that the large stability of the $Ti_{1-x}Al_xH_y$ systems is a consequence of the large charge transfer between the sites, resulting in a partly ionic bonding.

After discarding a possible link between embrittlement and a reduced stability, we investigated the correlation between reduced mechanical strength and the elastic response of the different $Ti_{1-x}Al_xH_y$ systems. Our results for the bulk modulus are also summarized in Table I. These results confirm that, with its bulk modulus being more than twice that of its pure constituents, Ti_3Al is indeed much stiffer and stronger than pure bulk Ti or Al. Our results indicate that the presence of hydrogen has only a negligible effect on the bulk modulus of all $Ti_{1-x}Al_x$ systems investigated. Hence we conclude that the embrittlement in $Ti_{1-x}Al_xH_y$ systems is not reflected in changes of the bulk modulus.

Finally, we investigated the elastic response of $Ti_{1-x}Al_xH_y$ systems with respect to applied shear stress, noting that a decreasing shear modulus C_{44} would likely enhance the creation and mobility of dislocations and hence lead to a locally enhanced plasticity. We calculated C_{44} using total energy differences, and verified the linearity of the response for small deformations. Due to the large size of the unit cells (which are implicitly assumed to be orthogonal in our bulk LDA code) in distorted single crystals, we performed the calculations of C_{44} on small $Ti_{1-x}Al_xH_y$ clusters with a hcp geometry. There, we were not restricted to periodic structures, and could consider even very small deformations along the x direction perpendicular to the c axis. A good agreement between cluster-based and bulk-based calculations, verified in the case of Al(fcc), indicates that our results are not dominated by surface effects.

Our results for the elastic constant C_{44} in $Ti_{1-x}Al_xH_y$ systems, for a shear of the (0001) planes in response to a shear stress along the [1000] direction, are summarized in Table I. As in the case of the bulk modulus, we find that also the shear modulus of Ti increases significantly upon alloying with Al. In strong contrast to the bulk modulus, however, we find a strong *decrease* of the shear modulus in $Ti_{1-x}Al_x$ alloys upon hydrogen loading, namely, from $C_{44}(Ti_3Al)$= 101 GPa to $C_{44}(Ti_3AlH_4)$= 67 GPa. We conclude that the decrease of the shear modulus C_{44} of Ti, which occurs only while hydrogen and aluminum are simultaneously present in the metal matrix, is closely related to the reduced mechanical strength of $Ti_{1-x}Al_x$ systems upon hydrogen loading. This interpretation is also consistent with our result of Table I that, in absence of aluminum, the introduction of H into the Ti matrix leads to an *increase* of the shear modulus from C_{44}(Ti)= 43 GPa to C_{44}(TiH)= 52 GPa, in close agreement with the analogous behavior observed in NbH_y systems.[42]

Less easy to interpret are our results for the elastic response to applied shear stress along the $[11\bar{2}0]$ direction, which results in a shear of the $(1\bar{1}00)$ planes. Even though these planes are known to form the preferential slip system in the $Ti_{1-x}Al_x$ alloys,[43] our preliminary results indicate relatively large values of C_{44}, ranging from C_{44}(Ti)= 137 GPa to $C_{44}(Ti_3Al)$= 129 GPa and $C_{44}(Ti_3AlH_4)$= 143 GPa.

The hydrogen-induced reduction of the shear modulus along the [1000] direction in $Ti_{1-x}Al_x$ alloys, and the anticipated increased mobility of dislocations in these systems, are consistent with the "hydrogen-enhanced local plasticity" (HELP) mechanism of failure. This microscopic mechanism had originally been proposed by Beachem[37] to explain fracture of hydrogen-loaded steel under tensile stress, and has been more recently used to explain a similar behavior in other high-strength Al-based alloys.[39] In systems under tensile stress, defects are often present near strain singular points such as crack tips. The initial growth and propagation of these cracks is accelerated by a rapid local accumulation of hydrogen, which leads to a local ductility enhancement near these crack tips. Under tensile stress, fracture propagation is accelerated at such hydrogen-saturated weak links, while the bulk of the matrix is essentially unperturbed. This mechanism leads to a fracture morphology which is indistinguishable from brittle fracture, since brittle fracture implies no crystal shape changes outside the crack region, whereas a typical ductile fracture is accompanied by large-scale shape deformations.

The next important problem is to determine the electronic origin of the strong reduction of the shear modulus in $Ti_{1-x}Al_x$ alloys upon hydrogen loading, which we linked to the hydrogen embrittlement of these systems. In particular, we want to identify the electronic properties which would reflect changes of C_{44}.

One of the most suitable quantities to reflect bonding changes in a given system is the electronic density of states. Indeed, we find the electronic density of states of Ti_3Al, shown in Fig. 8(a), to differ significantly from that of Ti_3AlH_4, given in Fig. 8(b). Even though the increased population of s states, apparent from the comparison of Figs. 8(a) and 8(b), may be indicative of a decreased bonding anisotropy which would cause a lowering of C_{44}, a definitive conclusion along these lines is difficult to make based on these results.

The difficulty of extracting information about the shear modulus from the density of states results from the fact that bonding anisotropy is only very indirectly reflected in this quantity. From this point of view, an observable which should reflect more directly the bonding anisotropy is the spatial distribution of electrons. We would expect the most pronounced changes due to the presence of hydrogen to occur near a substitutional Al impurity in bulk Ti(hcp). Our corresponding results for a $Ti_{12}Al$ and a $Ti_{12}AlH_6$ cluster are shown in Figs. 3(b) and 7(b), respectively. These results indicate the predominant localization of the electronic charge on the atomic sites. Even the more detailed charge density contour plot in Fig 3(c) for the hydrogen-free system does not show any significant charge accumulation in the bond regions, or a bonding anisotropy of the charge density. Hence we find no simple indication of a reduced shear modulus in the total charge density distribution.

A first indication of significant electronic structure differences between the hydrogen-free Ti_3Al alloy, which has a large shear modulus, and the hydrogen-loaded Ti_3Al alloy, which has a low shear modulus, was observed in the Mulliken populations of the sites. Our results, presented in Table III, show that in all the systems investigated in this study, hydrogen always carries a small negative excess charge, while Ti always carries a small positive net charge. Of particular interest, however, is a sign reversal of the net charge on the Al site, depending on whether or not hydrogen is present in the metal matrix. We can easily imagine that a partial ionic bonding between oppositely charged Al and Ti sites may provide additional stabilization within the hydrogen-free system with respect to shear distortions. This effect is absent in the hydrogen-loaded Ti_3Al alloy where all metal sites carry a net positive charge. Hence on the electronic level we may tentatively link the same sign of the excess charge on the metal impurity and its neighbors in the matrix with a propensity towards lowering the shear modulus.

Perhaps more instructive than the net charge on the

individual sites, or the distribution of the total charge density, should be an inspection of the valence charge distribution. In clusters, as well as in molecules, it is the charge distribution in the highest occupied molecular orbital (HOMO) which reflects the bonding nature, the stability, and particularly weak links in the system. The HOMO charge distribution in the hexagonal clusters $Ti_{13}H_6$ and $Ti_{12}AlH_6$ is shown in Figs. 9(a) and 9(b), respectively. The HOMO of the Al-free system displays lobes of charge in the direction of the c axis which connect as bridges the (0001) planes in the structure. Such valence charge bridges connecting the (0001) planes are even stronger in the hydrogen-free ordered alloy Ti_3Al with a large value of C_{44}, and near substitutional Al impurities in Ti, represented by a $Ti_{12}Al$ cluster. On the other hand, as shown in Fig. 9(b), these lobes or bridges are absent near substitutional Al impurities in the hydrogen-loaded Ti matrix. Hence in the particular case of $Ti_{1-x}Al_xH_y$ alloys we interpret a connected three-dimensional mesh of charge density in the HOMO, such as that found for $Ti_{13}H_6$ and $Ti_{12}Al$, as an indication for a shear-resistant structure. On the other hand, presence of charge-depleted (0001) planes in the HOMO charge distribution, such as in the case of $Ti_{12}AlH_6$, can be plausibly connected with a lowered resistance towards shear along a direction perpendicular to the c axis.

VII. CONCLUSIONS

We used a combination of different *ab initio* computational methods in an attempt to understand the adverse effect of hydrogen on the mechanical stability of $Ti_{1-x}Al_x$ alloys, also known as hydrogen embrittlement. Our studies focused on the equilibrium structure and the elastic constants of bulk Ti, Al, the ordered alloy Ti_3Al, as well as their hydrides. Calculations for ordered systems were performed using a bulk method with local orbitals and *ab initio* pseudopotentials. Results for the electronic structure of Ti near atomic vacancies, substitutional Al, and interstitial H impurities were obtained using the cluster approach and the linear muffin-tin orbitals in the atomic spheres approximation (LMTO-ASA) –Green function formalism.

The complementary results of these calculations indicate that the reduced stability of $Ti_{1-x}Al_x$ alloys is reflected in a significant reduction of the shear modulus C_{44} of these systems upon hydrogen loading. On the electronic level, we found the decrease of the shear modulus to be reflected in the distribution of the electrons at the top of the valence band, or in the HOMO orbital in the corresponding clusters. While this valence charge forms a relatively rigid mesh in Ti_3Al and TiH, we observe a valence charge depletion in the (0001) planes of the lattice in the case that both Al and H are present in the Ti matrix. It appears as plausible that this valence charge depletion may reduce the resistance of hydrogen-loaded $Ti_{1-x}Al_x$ alloys towards shear perpendicular to the c axis. Consequently, these planes could act as preferential gliding planes in perfect crystals or preferential planes for dislocation motion in imperfect crystals, resulting in a plastic deformation of the titanium matrix near aluminum impurities surrounded by hydrogen. This interpretation would be consistent with the hydrogen-enhanced local plasticity mechanism discussed above. We note that all our theoretical findings, as well as their above interpretation, are consistent with the experimental observation that hydrogen embrittlement occurs only in the presence of Al in the Ti matrix.[10]

Of course, these static results, obtained within the linear response regime, are far from describing the complex nature of fracture in realistic systems. Nevertheless, they provide us with an understanding of the atomic-level processes which are likely to occur in hydrogen-loaded $Ti_{1-x}Al_x$ systems subjected to tensile stress, and will form a basis for future dynamical calculations. Such studies are likely to address the effect of extended stacking faults and microvoids on the overall stability, the dynamics of dislocation motion, as well as the mechanism of crack propagation in these alloys. We believe that a fundamental understanding of atomic- and electronic-level processes linked with the adverse effect of hydrogen on the mechanical stability of $Ti_{1-x}Al_x$ systems could prove to be very useful in the exploration of materials treatment techniques and additives which would inhibit or suppress hydrogen embrittlement in these important alloys.

ACKNOWLEDGMENTS

We thank Professor Howard Birnbaum, Professor Sidney Yip, and Professor Marc De Graef for useful discussions and helpful comments. This study has been supported by the Office of Naval Research under Grant No. N00014-90-J-1396.

[1] A. J. Sedriks, J. A. S. Green, and P. W. Slattery, in *The Science Technology and Application of Titanium*, edited by R. Jaffee and N. Promisel (Pergamon, Oxford, 1970), pp. 283–291.
[2] Y.-W. Kim and D. M. Dimiduk, J. Met. **43**, 40 (1991).
[3] H. A. Lipsitt, D. Shechtman, and R. E. Schafrik, Metall. Trans. **6A**, 1991 (1975).
[4] T. Kawabata, T. Kanai, and O. Izumi, Acta Metall. **33**, 1355 (1985); G. Hug, A. Loiseau, and A. Lasalmonie, Philos. Mag. A **54**, 47 (1986).
[5] B. F. Greenberg, V. I. Anisimov, Y. N. Gornostirev, and G. G. Taluts, Scr. Metall. **22**, 859 (1988).
[6] M. Morinaga, J. Saito, N. Yukawa, and H. Adachi, Acta Metall. **38**, 25 (1990).
[7] C. L. Fu and M. H. Yoo, Philos. Mag. Lett. **62**, 159 (1990).
[8] *Hydrogen in Metals I and II*, edited by G. Alefeld and J. Völkl, Topics in Applied Physics Vols. 28 and 29 (Springer-Verlag, Berlin, 1978).
[9] J. A. S. Green and A. J. Sedriks, Corrosion **28**, 226 (1972).
[10] A. J. Sedriks and J. A. S. Green, J. Met. **23**, 48 (1971).

[11] A. J. Sedriks, J. A. S. Green, and P. W. Slattery, Corrosion **24**, 172 (1968).
[12] D. Tománek, Z. Sun, and S. G. Louie, Phys. Rev. B **43**, 4699 (1991).
[13] H. P. Leckie, Corrosion **23**, 187 (1967).
[14] For a review, see A. C. Switendick, in *Hydrogen in Metals I* (Ref. 8).
[15] P. Hohenberg and W. Kohn, Phys. Rev. **136**, B864 (1964); W. Kohn and L. J. Sham, *ibid.* **140**, A1133 (1965).
[16] L. Hedin and B. J. Lundqvist, J. Phys. C **4**, 2064 (1971).
[17] C. T. Chan, D. Vanderbilt, and S. G. Louie, Phys. Rev. B **33**, 2455 (1986); C. T. Chan, D. Vanderbilt, S. G. Louie, and J. R. Chelikowsky, *ibid.* **33**, 7941 (1986).
[18] D. R. Hamann, M. Schlüter, and C. Chiang, Phys. Rev. Lett. **43**, 1494 (1979).
[19] D. J. Chadi and M. L. Cohen, Phys. Rev. B **8**, 5747 (1973).
[20] P. Jund and C. Koenig, J. Magn. Magn. Mater. **119**, 279 (1993); **127**, 41 (1993).
[21] B. Delley, J. Chem. Phys. **92**, 508 (1990).
[22] U. von Barth and L. J. Hedin, J. Phys. C **5**, 1629 (1972).
[23] A standard, but not unique, reference is V. L. Moruzzi, J. F. Janak, and A. R. Williams, *Calculated Electronic Properties of Metals* (Pergamon Press, New York, 1978).
[24] Our LMTO-ASA result for the bulk lattice constant of Al(fcc) $a = 7.60$ a.u. is in perfect agreement with the previously published results of Ref. 23 and agrees even better with the experimental data than our pseudopotential calculations with a local basis. However, LMTO calculations of the elastic response often give a large discrepancy with the experimental data. As an example, the bulk modulus of Al(fcc) $B = 80$ GPa of Ref. 23 is in a much larger disagreement with the experimental result $B_{\rm expt} = 73$ GPa than our value $B = 71$ GPa.
[25] We define the cohesive energy with respect to *isolated* atoms.
[26] We present the density of states per formula unit, per spin, and per eV. Consequently, the integral over the occupied density of states gives half the total number of electrons.
[27] I. R. Lane and J. L. Cavallaro, Am. Soc. Test. Mater. Spec. Tech. Publ. **432**, 147 (1968).
[28] *Binary Alloy Phase Diagrams*, edited by T. B. Massalski, H. Okamoto, P. R. Subramanian, and L. Kacprzak, 2nd ed. (ASM International, Materials Park, OH 1990), Vol. 1, p. 226.
[29] The formation energy of Ti_xAl (with respect to the elements in their standard state) is defined by $E_{\rm form}(Ti_xAl) = E_{\rm total}(Ti_xAl) - xE_{\rm total}(Ti\ bulk) - E_{\rm total}(Al\ bulk)$, where $E_{\rm total}$ are energies of pseudoatoms and systems of pseudoatoms. An equivalent expression is $E_{\rm form}(Ti_xAl) = E_{\rm coh}(Ti_xAl) - xE_{\rm coh}(Ti\ bulk) - E_{\rm coh}(Al\ bulk)$.
[30] *Structure Data of Elements and Intermetallic Phases*, edited by K.-H. Hellwege and A. M. Hellwege, Landolt-Börnstein, New Series, Group III, Vol. 6 (Springer, Berlin, 1971), p. 279.
[31] The formation energy of XH_n (with respect to the elements in their standard state) is defined by $E_{\rm form}(XH_n) = E_{\rm total}(XH_n) - E_{\rm total}(X\ bulk) - (n/2)E_{\rm total}(H_2\ molecule)$, where $E_{\rm total}$ are energies of pseudoatoms and systems of pseudoatoms. We use for the energy of the H_2 pseudomolecule $E_{\rm total}(H_2\ molecule) = 2E_{\rm total}(H\ atom) + D(H_2) = -31.27$ eV, based on $E_{\rm total}(H\ atom) = -13.26$ eV (Ref. 12) and the experimental value for the H_2 dissociation energy $D(H_2) = 4.75$ eV (Ref. 44).
[32] W. M. Mueller, J. P. Blackledge, and G. G. Libowitz, *Metal Hydrides* (Academic Press, New York, 1968).
[33] M. Gupta, Solid State Commun. **29**, 47 (1979).
[34] N. I. Kulikov, V. N. Borzunov, and A. D. Zvonkov, Phys. Status Solidi B **86**, 83 (1978).
[35] Experimental value for Ti_3AlH_x (for $x \geq 1.5$), based on an assumed fcc structure, obtained from *Structure Data of Elements and Intermetallic Phases* (Ref. 30), Pt. 14a, p. 322.
[36] *Hydrogen Damage*, edited by C.D. Beachem (American Society for Metals, Metals Park, OH, 1977); *Atomistic of Fracture*, Vol. 5 of *NATO Conference Series VI: Materials Science*, edited by R. M. Latanision and J. R. Pickens (Plenum, New York, 1983).
[37] C. D. Beachem, Metall. Trans. **3**, 437 (1972).
[38] T. Tabata and H. K. Birnbaum, Scr. Metall. **18**, 231 (1984).
[39] G. M. Bond, I. M. Robertson, and H. K. Birnbaum, Acta Metall. **35**, 2289 (1987).
[40] S. P. Lynch, J. Mater Sci. **21**, 692 (1986).
[41] J. Wang, S. Yip, S. R. Phillpot, and D. Wolf, Phys. Rev. Lett. **71**, 4182 (1994).
[42] F. M. Mazzolai and H. K. Birnbaum, J. Phys. F **15**, 507 (1985).
[43] S. A. Court, J. P. A. Löfvander, M. H. Loretto, and H. L. Fraser, Philos. Mag. A **61**, 109 (1990).
[44] B. Stoicheff, Can. J. Phys. **35**, 730 (1957).

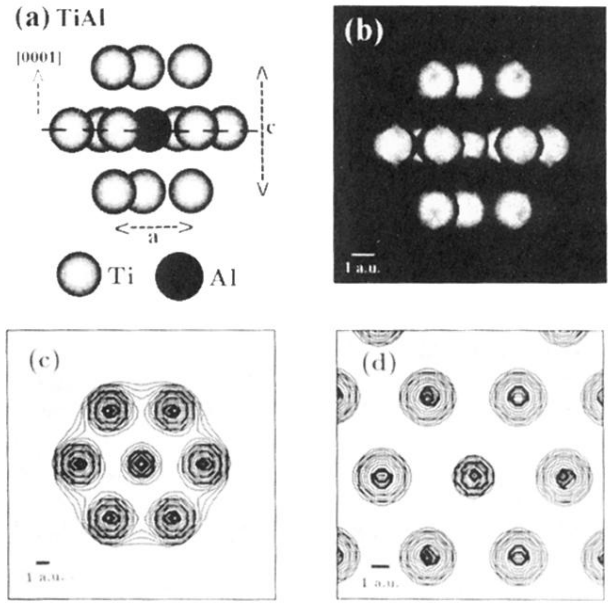

FIG. 3. Geometry and charge distribution in a very dilute TiAl alloy, represented by Ti(hcp) with a substitutional Al impurity. (a) Geometry of the $Ti_{12}Al$ core cluster. (b) Three-dimensional (3D) representation of the total charge density surface in the $Ti_{12}Al$ cluster, corresponding to $\rho = 0.1\ e^-/\text{a.u.}^3$, calculated using the DMOL all-electron cluster method. (c) Results of the same calculation, presented as a 2D contour plot in the (0001) plane, which is shown by the dashed line in (a) and contains the Al impurity. (d) Total charge density in the dilute TiAl alloy, calculated using the LMTO–ASA–Green-function method, and represented in the same manner and geometry as in (c). The ratio of two consecutive contours in (c) and (d) is $\rho(n+1)/\rho(n) = 1.5$.

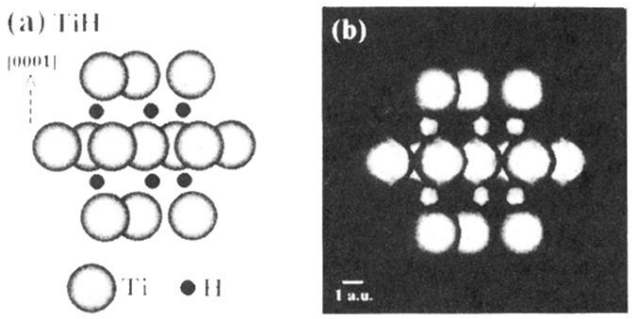

FIG. 5. Geometry and charge distribution in TiH, with hydrogen atoms occupying the octahedral interstitial sites of the hcp lattice. (a) Geometry of a $Ti_{13}H_6$ core cluster. (b) 3D representation of the total charge density surface in the $Ti_{13}H_6$ cluster, corresponding to $\rho = 0.1\ e^-/\text{a.u.}^3$, calculated using the DMOL all-electron cluster method.

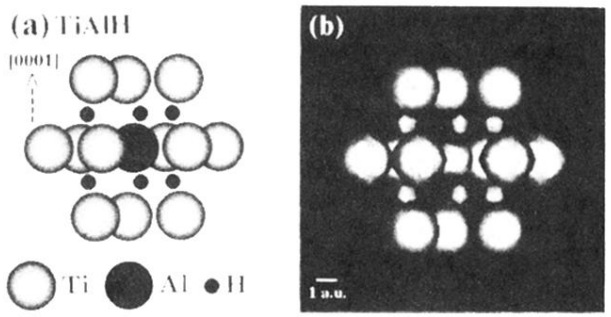

FIG. 7. Geometry and charge distribution in the hydride of a very dilute TiAl alloy, represented by a Ti(hcp) matrix with a substitutional Al impurity and hydrogen atoms occupying the octahedral interstitial sites of the hcp lattice. (a) Geometry of a $Ti_{12}AlH_6$ core cluster. (b) 3D representation of the total charge density surface in the $Ti_{12}AlH_6$ cluster, corresponding to $\rho = 0.1\ e^-/\text{a.u.}^3$, calculated using the DMOL all-electron cluster method.

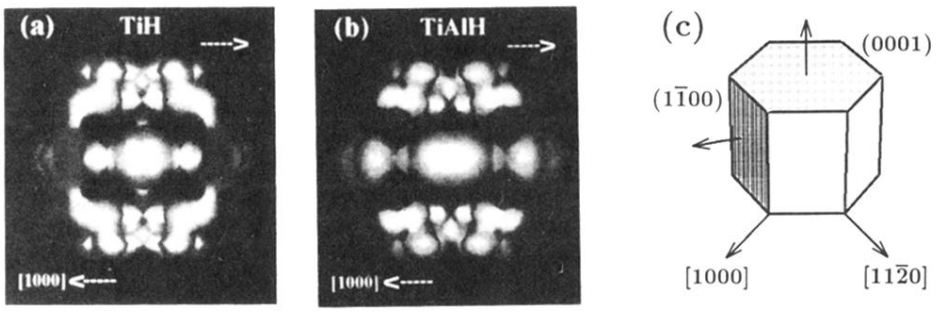

FIG. 9. Charge distribution in the highest occupied molecular orbitals (HOMO's) of (a) $Ti_{13}H_6$ and (b) $Ti_{12}AlH_6$ clusters, both based on the bulk Ti(hcp) structure, calculated using the DMOL all-electron cluster method. A 3D representation of the total charge density surface in (a) and (b) is shown at the value $\rho = 0.001\ e^-/\text{a.u.}^3$. The geometry has been given in Figs. 5(a) and 7(a), respectively. The arrows indicate possible applied shear stress. (c) Schematic drawing of the shear directions and gliding planes in $Ti_{1-x}Al_x$ systems.